J. Phys. B: At. Mol. Opt. Phys. **24** (1991) 1683–1694. Printed in the UK

Charge transfer and excitation in proton–helium collisions

H A Slim, E L Heck, B H Bransden and D R Flower
Physics Department, The University, Durham DH1 3LE, UK

Received 25 October 1990, in final form 14 January 1991

Abstract. Using the semiclassical impact parameter method, we have computed cross sections for excitation of He by H^+ and for one-electron charge transfer, the collision energy being in the range from 10–235 keV. A basis of travelling atomic orbitals was used, comprising 11 states on the helium target and 29 states on the projectile. Results are presented both including and neglecting the effects of two-electron exchange arising from the Pauli exclusion principle. Comparison is made with measurements of the density matrix elements relating to capture into the $n = 2$ and $n = 3$ states of hydrogen and with measurements of the cross sections for excitation of the 1s2s ^{1}S and 1s2p ^{1}P levels of helium. Comparison is also made with relevant calculations, including recent computations based upon a one-electron model.

1. Introduction

Theoretical studies of charge transfer and excitation in H^+–He collisions have been stimulated by the existence of a substantial body of experimental data pertaining to this system. The recent measurements by Ashburn *et al* (1989, 1990) and Brower and Pipkin (1989) enable the elements of the density matrix for capture into the $n = 3$ states of hydrogen to be derived. Comparison between theory and experiment at this level of sophistication may be expected to provide valuable insights into the nature of the physical processes involved.

Proton–helium is an archetypal system for the study of the effects of two-electron exchange, arising from the Pauli exclusion principle. Early theoretical work by Green *et al* (1965) and Sin Fai Lam (1967) showed that the total (one-) electron capture cross section was dominated by the H(1s) state, a result which has received ample confirmation since that time. Subsequent calculations by Kimura and Lin (1986) were based on a hybrid atomic orbital (AO)/molecular orbital (MO) approach, in the range of proton energies $1 \leqslant E \leqslant 100$ keV. In the inner, MO, region an electron translation factor (ETF) was incorporated in the wavefunction to ensure the translational invariance (origin independence) of the results, and the solutions matched to travelling atomic orbitals at an appropriate value of the time, t, the integration variable. States correlating with He $1s^2$, 1s2s, 1s2p and H 1s, 2s, 2p, 3p in the outer, AO, region were included in the expansion.

A larger, 19-state basis was used in the AO calculations of Jain *et al* (1987a, b). In this case, the helium atom was approximated by a single electron wavefunction, determined by an effective, central potential. Effects arising from the exchange of the two electrons present in the real system are taken only partially into account in this approximation, through the effective potential. Very recently, Shingal and Lin (1990)

0953-4075/91/071683+12$03.50

have extended this approach by including a much larger (64-)state basis of travelling atomic orbitals.

Our own work has been directed towards obtaining results for excitation and charge transfer, with full allowance for the effects of two-electron exchange. In an earlier letter (Slim *et al* 1990), we compared our results for capture into the H($n=3$) states with the measurements of Ashburn *et al* (1989, 1990) and Brower and Pipkin (1989). A basis comprising travelling orbitals representing 33 states was used in these computations. The present paper contains a more detailed account of these calculations and a comprehensive presentation of the results which have been obtained with a basis set larger than the previous 33 states. Comparison is made with measurements of cross sections for charge transfer and excitation and with other theoretical results, including the recent effective potential calculations by Shingal and Lin (1990).

2. Theoretical model and computational techniques

The semiclassical, impact-parameter method has been used to solve the proton-helium scattering problem. This method is known to be valid in the keV energy range, where straight-line trajectories are a sufficiently accurate approximation.

The time-dependent Schrödinger equation may be reduced to a set of coupled differential equations for the transition amplitudes, $a_{ij}(b, t)$, and integrated with respect to time, t, for a given value of the impact parameter, b. As in the case of H-H scattering (Shingal *et al* 1987, 1989), the matrix elements, which are integrals over electronic coordinates, were evaluated numerically in the body-fixed frame, where the H^+-He^{2+} internuclear vector is the z axis (appendix). A rotation is then performed into the space-fixed frame, where the z axis is the direction of incidence of the H^+ projectile. The electronic wavefunctions incorporated plane-wave translation factors, known to be required to ensure the translational invariance of the solutions (Bates and McCarroll 1958). A final numerical integration, with respect to impact parameter, yields cross sections from the initial to all possible final states.

In the present work, the two-electron exchange matrix elements were evaluated without further approximation; in this sense, electron exchange was treated 'exactly'. The calculations involved a number of technical innovations, as the programs were run on a Meiko Computing Surface, a parallel processor comprising Inmos T-800 transputers, configured in a daisy chain. The FORTRAN code has been implemented on the Computing Surface within the FORTNET Occam harness of Allan *et al* (1990). The combination of the computational power provided by the Computing Surface and the storage available (for the matrix elements) on a 700 Mbyte front-end disk has enabled calculations to be performed of a size and accuracy which, we believe, significantly exceed anything previously achieved for the H^+-He problem.

The basis set on the He (target) nucleus comprised the ground $1s^2\ ^1S$ state, the singly excited 1s2s ^1S and 1s2p ^1P states, together with the $2s^2\ ^1S$, 2s2p ^1P, $2p^2\ ^1S$ and ^1D autoionizing states (11 states in total), expanded in terms of Slater orbitals as prescribed by Fritsch and Lin (1988). A larger basis of 29 states was placed on the proton (projectile), consisting of the 1s, 2s, 2p, 3s, 3p, 3d, 4s, 4p, 4d states, together with four s, three p and one d pseudostate. These were obtained by diagonalizing the hydrogen Hamiltonian on the set of Slater functions specified in table 1.

The coupled equations were integrated with respect to the scaled variable, $z = vt$, where v is the relative velocity of the projectile and the target, from a large negative

Table 1. Parameters of the 22 Slater functions, $r^p e^{-\lambda r}$, used to construct hydrogen eigenstates with orbital angular momenta $l=0, 1$ and 2. The energies of the subset of the eigenstates which was included in the scattering calculation are listed in the last column.

l	p	λ	Eigenenergies (Hartree)
0	0	1	−0.5
	0	1/2	−0.125
	1	1/2	−0.05556
	0	1/3	−0.03125
	1	1/3	0.01033
	2	1/3	0.07126
	0	1/4	0.2963
	1	1/4	1.894
	2	1/4	
	3	1/4	
1	1	1	−0.125
	1	1/2	−0.05556
	1	1/3	−0.03125
	2	1/3	0.01779
	1	1/4	0.1321
	2	1/4	0.8097
	3	1/4	
	1	1/5	
2	2	1/2	−0.05556
	2	1/3	−0.03125
	2	1/4	0.06827
	3	1/4	

to a large positive value of z. In the present calculations the initial and final points were $z=\pm 69a_0$. At still larger values of z, the only significant couplings which remain involve the dipolar interactions between the degenerate nl states of hydrogen, within each n manifold. Following Cheshire *et al* (1970), the variation of the transition amplitudes for $z>69a_0$, arising from these long-range interactions, may be expressed in analytic form, enabling their extrapolation to infinite internuclear separation.

3. Results and discussion

We shall divide the presentation of our results into sections on charge transfer and on direct collisional excitation, with the emphasis on the former. The initial state of the system at infinite separation of the nuclei, is taken to be H^+–$He(1s^2\ ^1S)$, so only those states with an overall singlet spin symmetry need to be taken into account.

3.1. Charge transfer

From the amplitudes for charge transfer into the individual states of hydrogen may be calculated the complete density matrix, the diagonal elements of which are proportional to the cross sections, σ_{nlm}. We consider first the information which may be derived from σ_{nlm}.

Table 2. Partial cross sections (10^{-16} cm^2) for capture into the $n = 1$, 2 and 3 states of hydrogen in H^+-He collisions, as functions of the collision energy, E. The upper entry is the exact result, the lower is that obtained on neglecting two-electron exchange. Also given is the cross section for capture to all (real and pseudo) bound states of hydrogen, σ_{bound}, which is compared with the measurements of Shah *et al* (1989), made at slightly different energies (in general). The total cross section, σ_{total}, which is the sum of contributions from bound and pseudocontinuum states, is presented last.

	E (keV)								
	10	20	30	40	50	60	80	100	135
1s	1.29	2.15	1.98	1.54	1.14	8.33 (−1)	4.54 (−1)	2.60 (−1)	1.11 (−1)
	1.79	2.55	2.18	1.70	1.28	9.55 (−1)	5.33 (−1)	3.06 (−1)	1.28 (−1)
2s	2.51 (−2)	3.51 (−2)	8.51 (−2)	1.13 (−1)	1.13 (−1)	9.75 (−2)	6.34 (−2)	3.98 (−2)	1.81 (−2)
	4.64 (−2)	4.36 (−2)	8.83 (−2)	1.20 (−1)	1.23 (−1)	1.10 (−1)	7.44 (−2)	4.70 (−2)	2.08 (−2)
2p	1.58 (−2)	2.84 (−2)	3.21 (−2)	2.61 (−2)	2.07 (−2)	1.59 (−2)	9.02 (−3)	5.31 (−3)	2.25 (−3)
	5.03 (−2)	7.14 (−2)	4.87 (−2)	2.60 (−2)	1.51 (−2)	1.05 (−2)	6.80 (−3)	4.51 (−3)	2.11 (−3)
3s	4.40 (−3)	7.43 (−3)	1.70 (−2)	2.70 (−2)	3.02 (−2)	2.83 (−2)	1.96 (−2)	1.24 (−2)	5.79 (−3)
	1.11 (−2)	1.55 (−2)	1.83 (−2)	2.85 (−2)	3.29 (−2)	3.19 (−2)	2.31 (−2)	1.48 (−2)	6.74 (−3)
3p	2.98 (−3)	7.42 (−3)	1.42 (−2)	1.14 (−2)	8.53 (−3)	6.72 (−3)	3.62 (−3)	2.07 (−3)	7.75 (−4)
	1.56 (−2)	2.11 (−2)	1.96 (−2)	1.19 (−2)	6.54 (−3)	4.33 (−3)	2.43 (−3)	1.60 (−3)	7.58 (−4)
3d	1.10 (−3)	1.81 (−3)	2.12 (−3)	1.37 (−3)	7.93 (−4)	6.00 (−4)	2.78 (−4)	1.16 (−4)	3.61 (−5)
	3.63 (−3)	3.47 (−3)	2.06 (−3)	1.37 (−3)	8.47 (−4)	6.05 (−4)	2.63 (−4)	1.04 (−4)	3.76 (−5)
σ_{bound}	1.34	2.24	2.15	1.74	1.33	9.96 (−1)	5.60 (−1)	3.26 (−1)	1.40 (−1)
	1.93	2.72	2.37	1.90	1.48	1.13	6.51 (−1)	3.81 (−1)	1.61 (−1)
Shah *et al*	1.13 ± 0.06	1.69 ± 0.08	1.71 ± 0.08	1.28 ± 0.06	1.01 ± 0.05	0.80 ± 0.05	0.400 ± 0.019	0.274 ± 0.014	
σ_{total}	1.38	2.33	2.40	2.18	1.91	1.70	1.38	1.10	7.95 (−1)
	2.05	3.01	2.72	2.36	2.04	1.83	1.50	1.20	8.72 (−1)

3.1.1. Partial and total charge transfer cross sections. In table 2 are given the partial cross sections, σ_{nl}, for electron transfer into nl subshells of the hydrogen atom, up to and including 3d, together with their sum. For each transition, there are two entries, the upper being the 'exact' result, including two-electron exchange, the lower being obtained on neglecting electron exchange.

It may be seen from table 2 that electron exchange is a significant phenomenon over the entire energy range considered, $10 \leqslant E \leqslant 135$ keV, increasingly so as the collision energy falls. At the lowest energies considered, the neglect of electron exchange leads to large errors in the cross sections for charge transfer into certain excited states of hydrogen. As expected, charge transfer is dominated by H(1s) capture, particularly at low energies.

Also given in table 2 are the total cross sections for one-electron capture by the proton, obtained as the sums of the contributions from all bound states of the hydrogen atom, including negative-energy pseudostates. The grand total, including *positive*-energy pseudostates, is also given. The differences between these pairs of numbers provide a measure of the contribution of charge transfer into the continuum to the single ionization cross section. The measurements of Shah *et al* (1989) are included for comparison.

Compared with the measurements, the present calculations appear to overestimate the one-electron capture cross section; the discrepancies are much larger than the quoted experimental error bars. It is surprising to see differences of this magnitude between what are believed to be accurate measurements and calculations.

To investigate this discrepancy further, we rescaled our total capture cross section with a factor 0.78, obtained from a linear least-squares fit to the experimental data points. Around half of the rescaled theoretical values fell within the experimental error bars, and most other points just above or below. We note that Shah *et al* (1989) normalized their data to results from earlier experiments (Shah and Gilbody 1985, Stier and Barnett 1956), and this could have some bearing on the discrepancy. On the other hand, our basis set does not include any direct ionization channels on the helium centre. These might significantly affect the capture cross section to H(1s), which dominates the total capture cross section. Further work is being undertaken to clarify this issue. The theoretical results show the expected increase in the ionization cross section (due to charge transfer into the continuum), relative to the capture cross section, as the collision energy rises.

The partial capture cross sections which derive from the present (40 state) calculations agree to within 10% with our earlier (33 state) computations, and the level of agreement in the total capture cross section is even better, at about 5%; this lends some confidence in the convergence of these results with respect to extensions of the basis set.

In figure 1, we compare the partial cross sections for capture into the 3s, 3p and 3d states with the measurements of Lenormand (1976), Brower and Pipkin (1989) and Cline *et al* (1990), and the calculations of Jain *et al* (1987b). Our results for the 3s and 3p states agree better with the experiments than Jain *et al*, particularly in the region of the cross section maximum. Regarding the small 3d cross section, our calculations agree well with the more recent measurement by Brower and Pipkin and lie below the experimental data of Cline *et al* for $E > 40$ keV. The change of slope between 50 and 60 keV, present in the theoretical (and in two of the experimental) 3d cross sections, is attributable to the (dominant) $\bar{3}d_0$ partial cross section. Overall, we consider the comparisons made in figure 1 to be favourable to the present computations.

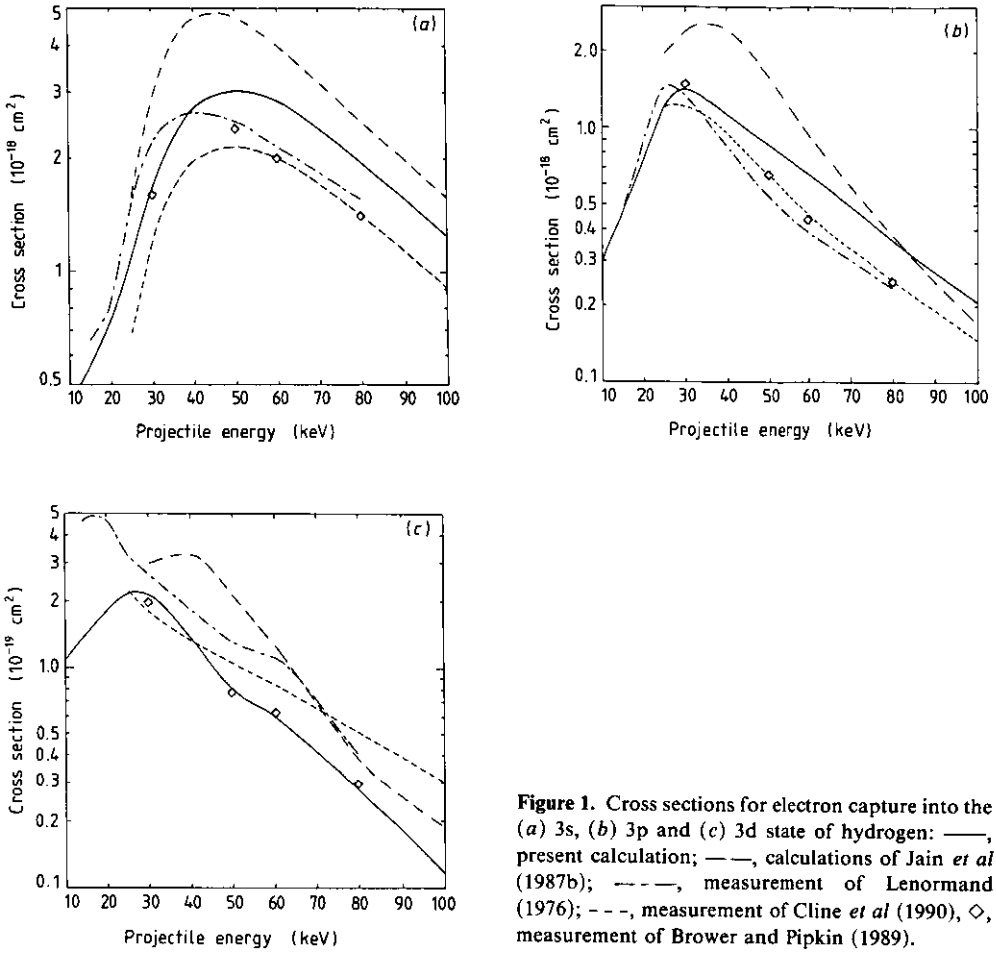

Figure 1. Cross sections for electron capture into the (*a*) 3s, (*b*) 3p and (*c*) 3d state of hydrogen: ——, present calculation; — —, calculations of Jain *et al* (1987b); — - —, measurement of Lenormand (1976); - - -, measurement of Cline *et al* (1990), ◇, measurement of Brower and Pipkin (1989).

3.1.2. Density matrix elements and related parameters. The charge transfer cross sections, considered above, were derived from integrals over impact parameter, of the type

$$\sigma_{ij}=2\pi\int_0^\infty |a_{ij}(b,\, t=\infty)|^2\,\mathrm{d}b$$

and their comparison with experiment provides a test of the diagonal elements of the density matrix. In an earlier letter (Slim *et al* 1990), we made a limited comparison of our calculations with the measurements by Ashburn *et al* (1989, 1990) and Brower and Pipkin (1989) of cross sections for capture into the *nlm* states of hydrogen. The basis set comprised those states of hydrogen up to and including 3d, together with a number of pseudostates. As mentioned above, we have since extended the basis to incorporate the exact 4s, 4p and 4d states, in order to improve the convergence of the $n=3$ scattering amplitudes and the associated density matrix elements.

In table 3 is presented the complete set of $n=3$ density matrix elements, obtained with the extended basis, together with the measurements of Ashburn *et al.* As it would be tedious to discuss the results for each parameter in turn, we shall restrict our comments to the salient features of this comparison.

Table 3. Measured (with error bars) and computed values of the density matrix elements for the states of the $n=3$ manifold in hydrogen, normalized to the H(3s) cross section.

	E (keV)						
	20	30	40	50	60	80	100
s_0	1.000 ± 0.082	1.000 ± 0.017	1.000 ± 0.008	1.000 ± 0.007	1.000 ± 0.008	1.000 ± 0.010	1.000 ± 0.009
	1.000	1.000	1.000	1.000	1.000	1.000	1.000
p_0	1.784 ± 0.060	0.757 ± 0.011	0.417 ± 0.005	0.282 ± 0.005	0.213 ± 0.005	0.164 ± 0.006	0.153 ± 0.005
	0.807	0.756	0.376	0.245	0.203	0.154	0.137
$p_{\pm1}$	0.740 ± 0.037	0.113 ± 0.006	0.034 ± 0.003	0.013 ± 0.003	0.007 ± 0.003	0.005 ± 0.003	0.003 ± 0.003
	0.096	0.038	0.023	0.019	0.017	0.016	0.015
d_0	0.576 ± 0.077	0.088 ± 0.013	0.051 ± 0.006	0.030 ± 0.006	0.030 ± 0.007	0.027 ± 0.008	0.027 ± 0.007
	0.154	0.103	0.041	0.020	0.016	0.010	0.006
$d_{\pm1}$	0.130 ± 0.055	0.019 ± 0.009	−0.003 ± 0.005	−0.001 ± 0.005	−0.005 ± 0.005	−0.007 ± 0.006	−0.009 ± 0.005
	0.042	0.009	0.004	0.003	0.002	0.002	0.002
$d_{\pm2}$	0.034 ± 0.013	0.010 ± 0.002	0.012 ± 0.001	0.011 ± 0.001	0.011 ± 0.001	0.011 ± 0.001	0.012 ± 0.001
	0.002	0.001	0.0007	0.0005	0.0004	0.0003	0.0003
$\mathrm{Re}(s_0p_0)$	0.373 ± 0.090	0.456 ± 0.018	0.397 ± 0.007	0.355 ± 0.006	0.324 ± 0.006	0.267 ± 0.008	0.241 ± 0.007
	0.174	0.535	0.449	0.410	0.391	0.342	0.318
$\mathrm{Im}(s_0p_0)$	−0.283 ± 0.086	−0.410 ± 0.017	−0.247 ± 0.007	−0.132 ± 0.006	−0.061 ± 0.007	0.019 ± 0.007	0.072 ± 0.007
	0.017	−0.350	−0.299	−0.095	−0.013	0.053	0.101
$\mathrm{Re}(s_0d_0)$	0.14 ± 0.11	0.143 ± 0.019	0.129 ± 0.008	0.090 ± 0.008	0.105 ± 0.009	0.063 ± 0.010	0.054 ± 0.009
	0.02	0.207	0.154	0.106	0.087	0.061	0.022
$\mathrm{Im}(s_0d_0)$	−0.29 ± 0.46	−0.230 ± 0.061	−0.142 ± 0.025	−0.154 ± 0.024	−0.090 ± 0.026	−0.057 ± 0.028	−0.052 ± 0.021
	−0.005	−0.066	−0.033	0.018	0.041	0.035	0.040
$\mathrm{Re}(p_0d_0)$	0.800 ± 0.032	0.218 ± 0.006	0.097 ± 0.003	0.057 ± 0.002	0.042 ± 0.002	0.025 ± 0.002	0.021 ± 0.002
	0.340	0.266	0.117	0.060	0.046	0.030	0.016
$\mathrm{Im}(p_0d_0)$	−0.090 ± 0.029	−0.021 ± 0.005	0.022 ± 0.002	0.026 ± 0.002	0.019 ± 0.002	0.015 ± 0.002	0.011 ± 0.002
	0.043	0.078	0.039	0.031	0.030	0.019	0.019
$\mathrm{Re}(p_{\pm1}d_{\pm1})$	0.291 ± 0.031	0.050 ± 0.006	0.014 ± 0.002	0.004 ± 0.002	0.000 ± 0.002	0.003 ± 0.002	−0.001 ± 0.002
	0.053	0.016	0.008	0.006	0.004	0.003	0.002
$\mathrm{Im}(p_{\pm1}d_{\pm1})$	−0.038 ± 0.012	0.009 ± 0.002	0.005 ± 0.001	0.002 ± 0.001	0.002 ± 0.001	0.003 ± 0.001	0.003 ± 0.001
	0.008	0.001	0.002	0.003	0.003	0.003	0.003
$\langle \underline{d} \rangle_z$	3.68 ± 0.21	4.63 ± 0.10	4.570 ± 0.057	4.333 ± 0.058	4.106 ± 0.060	3.500 ± 0.087	3.143 ± 0.069
	3.35	5.72	5.50	5.242	5.088	4.570	4.207
$\langle \underline{L} \times \underline{A} \rangle_{s,z}$	0.319 ± 0.054	0.642 ± 0.027	0.429 ± 0.016	0.219 ± 0.015	0.073 ± 0.017	−0.128 ± 0.019	−0.259 ± 0.020
	−0.152	0.407	0.381	0.111	−0.097	−0.244	−0.381

Some of the matrix elements are very small, which makes their reliable calculation or measurement difficult; this is true of the diagonal matrix elements for the $d_{\pm 1}$ and $d_{\pm 2}$ states, and of the imaginary parts of the off-diagonal elements. The error bars of the measurements increase towards lower energies, for which Ashburn *et al* themselves express reservations about the accuracy of the experimental results. At $E=20$ keV, the theoretical and experimental values bear little relation to each other. We believe that the error bars quoted in the table are conservative estimates of the combined uncertainties of the measurements and the fitting procedure. At $E=20$ keV, we suggest that the errors have been grossly underestimated. New measurements at low energies would be highly desirable. Overall, the level of agreement between theory and experiment is unsatisfactory, even at high energies. Deficiencies in the basis set may account for some, but not all of the discrepancies.

A comparison with our earlier 33 state calculations helps to shed some light on the question of basis set convergence. In general, the 40 state and 33 state results agree to about 20%, although there are exceptions, particularly in the imaginary parts of the off-diagonal matrix elements, where much larger discrepancies are encountered. As noted above, these matrix elements tend to be very small and so, not surprisingly, they are particularly sensitive to changes in the basis set.

Analogous quantities to those in table 3 may be computed for the $n=2$ manifold. Table 4 makes a comparison of the two coherence parameters which derive from the computations, with the values measured by De Serio *et al* (1988); the agreement may be seen to be generally good.

Table 4. The coherence parameters for the $n=2$ density matrix, normalized to the trace: a, measured by De Serio *et al* (1988); b, present work.

		E (keV)		
		135	186	235
$\mathrm{Re}(s_0p_0)$	a	0.20 ± 0.04	0.18 ± 0.04	0.17 ± 0.09
	b	0.19	0.12	0.10
$\mathrm{Im}(s_0p_0)$	a	0.12 ± 0.04	0.15 ± 0.04	0.13 ± 0.04
	b	0.15	0.19	0.20

In figure 2, we compare our computed values of the average electric dipole moment, $\langle \underset{\sim}{d} \rangle_z$, the symmetrized product, $\langle \underset{\sim}{L} \times \underset{\sim}{A} \rangle_{s,z}$, of the angular momentum and Runge–Lenz vectors, and the alignment parameter A_{20},

$$A_{20}=\frac{\sigma_1-\sigma_0}{\sigma_0+2\sigma_1}$$

for the $n=2$ manifold of hydrogen with the calculations of Shingal and Lin (1990) for $E \leqslant 100$ keV. Measurements of the dipole moment and of the alignment parameter are also plotted.

Figure 2(a) shows that our calculations of $\langle \underset{\sim}{d} \rangle_z$ follow the trend of the measurements at low energies and of the results of Shingal and Lin at high energies. The computations also agree on the general shape of the variation of $\langle \underset{\sim}{L} \times \underset{\sim}{A} \rangle_{s,z}$ with collision energy, although our results are larger than those of Shingal and Lin at high energies. Regarding the alignment parameter, our calculations fall well below the calculations of Shingal

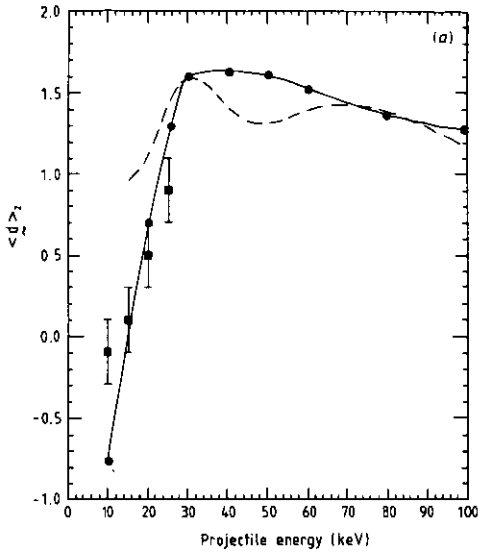

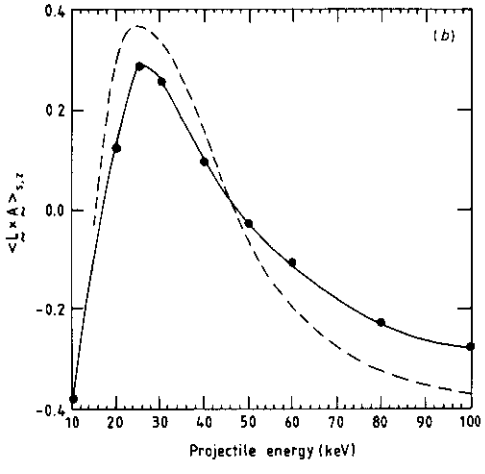

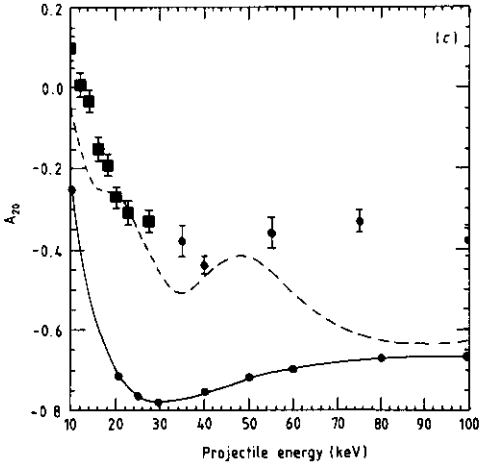

Figure 2. (*a*) Computed and measured values of the dipole moment for capture to the $n = 2$ manifold of hydrogen: —●—, present calculation, — —, calculation of Shingal and Lin (1990). The experimental points (with error bars) are as plotted by Shingal and Lin, following a private communication from Hippler (1990). (*b*) Computed values of $\langle \underset{\sim}{L} \times \underset{\sim}{A} \rangle_{s,z}$ for $n = 2$ capture: —●—, present results; — — Shingal and Lin (1990). (*c*) Alignment parameter, A_{20}, for capture to the 2p state of hydrogen: —●—, present calculation; — —, calculation of Shingal and Lin (1990); ●, measurements of Hippler *et al* (1986); ■, measurements of Teubner *et al* (1970).

and Lin at low energies and below the measurements at all energies, although the general shape is the same; this suggests that our computed values of the cross section for charge transfer into $2p_{\pm 1}$ are too small, relative to $2p_0$, a trend which can also be seen (for $3p_{\pm 1}$ and $3p_0$) in table 3.

As the energy increases, all cross sections are expected to scale according to the $1/n^3$ rule (Burgdörfer 1986), at least for n, the principal quantum number, sufficiently large. From table 2 we deduce the values $2^3\sigma_{2p} = 4.25 \times 10^{-18}$ and $3^3\sigma_{3p} = 5.59 \times 10^{-18}$ cm^2, at $E = 100$ keV, which indicate that application of this rule may be a reasonable approximation. Therefore, the value of the alignment parameter is not expected to vary greatly from $n = 2$ to $n = 3$. It is noteworthy that the measurements of Ashburn *et al* (1990), at $E = 100$ keV, yield (for $n = 3$) a value -0.94 for the alignment parameter, which falls *below* the theoretical values plotted in figure 2(*c*) and also below the measurement of Hippler *et al* (1986) for $n = 2$. Again, further measurements appear to be necessary to clarify the situation.

3.2. Excitation of helium

Measurements of the cross sections for production of the singly-excited 1s2s ^{1}S and 1s2p ^{1}P states of He by H^+ have been made by Kvale *et al* (1985), for the range of impact energies $25 \leqslant E \leqslant 100$ keV. Their results for the integral cross sections are compared with our calculations in table 5. The level of agreement between theory and experiment may be considered satisfactory, given the experimental error bars, and comparable with that achieved by AO-MO calculations of Kimura and Lin (1986). Comparison with the measured differential cross sections is deferred to a later publication, where differential cross sections for charge transfer will also be presented.

Table 5. Measured (with error bars) and computed cross sections (10^{-18} cm^2) for excitation of the 1s2s ^{1}S and 1s2p ^{1}P states of helium in He-H^+ collisions.

	E (keV)								
	20	25	30	40	50	60	75	80	100
1s2s ^{1}S		3.80 ± 1.30			6.85 ± 1.03		4.73 ± 0.69		5.36 ± 2.43
	4.95	5.83	5.98	6.23	6.69	6.02		2.95	5.06
1s2p ^{1}P		1.51 ± 0.82			7.80 ± 3.00		9.64 ± 0.92		13.7 ± 5.5
	3.14	2.85	2.96	5.10	8.04	8.56		10.7	15.3

The cross sections for production of the doubly-excited, autoionizing states 2s^2 ^{1}S, 2s2p ^{1}P, 2p^2 ^{1}S and ^{1}D are much smaller than the 1s2s ^{1}S and 1s2p ^{1}P cross sections, increasingly so with decreasing collision energy. We expect that the inclusion of a pseudostate representation of the $He^+(1s) + e^-$ continuum will modify the cross sections for excitation of the autoionizing states, and this is currently being investigated.

Acknowledgments

This work has received support from the SERC, in particular under the Computational Science Initiative. We are grateful to Rajiv Shingal for a preprint of his paper with C D Lin and to R Cline and W Westerveld for a preprint of their paper with J S Risley. We thank a referee for helpful comments.

Appendix

The electronic motion is with respect to a coordinate system which has a fixed orientation in space. The origin is located on the midpoint of the internuclear axis, represented by the vector $\boldsymbol{R}$, which points from the target nucleus (T) to the projectile nucleus (P), and the z axis is chosen parallel to the velocity of incidence of the projectile, v. The time dependence of the internuclear vector for a straight-line trajectory is $\boldsymbol{R} = \boldsymbol{b} + \boldsymbol{v}t$ where the impact parameter $\boldsymbol{b}$ is chosen along the x axis. The Hamiltonian for two electrons, moving in the time-dependent Coulomb field of two bare nuclei, P and T, with charges Z_P and Z_T, is, in atomic units,

$$H(\boldsymbol{r}_1, \boldsymbol{r}_2; t) = \sum_{i=1}^{2} \left(T_i - \frac{Z_T}{r_{iT}} - \frac{Z_P}{r_{iP}} \right) + \frac{1}{|\boldsymbol{r}_1 - \boldsymbol{r}_2|}. \tag{A1}$$

Here, for the ith electron, $T_i = -\frac{1}{2}\nabla_i^2$ is the kinetic energy, $\boldsymbol{r}_{i\mathrm{T}} = \boldsymbol{r}_i + \boldsymbol{R}/2$ and $\boldsymbol{r}_{i\mathrm{P}} = \boldsymbol{r}_i - \boldsymbol{R}/2$, where $\boldsymbol{r}_i$ is the electronic position vector in the coordinate system defined above.

In the variational solution of the time-dependent Schrödinger equation

$$\mathrm{i}\frac{\partial}{\partial t}\Phi(\boldsymbol{r}_1, \boldsymbol{r}_2; t) = H(\boldsymbol{r}_1, \boldsymbol{r}_2; t)\Phi(\boldsymbol{r}_1, \boldsymbol{r}_2; t) \tag{A2}$$

the electronic wavefunction, Φ, is expanded in a suitable set of basis functions, which in the present model are travelling atomic orbitals,

$$\begin{aligned}\Phi(\boldsymbol{r}_1, \boldsymbol{r}_2; t) = {} & \sum_{i=1}^{N_\mathrm{T}} a_i(t)\phi_i^{\mathrm{He}}(\boldsymbol{r}_{1\mathrm{T}}, \boldsymbol{r}_{2\mathrm{T}})w^{\mathrm{T}}(\boldsymbol{r}_1, t)w^{\mathrm{T}}(\boldsymbol{r}_2, t)\exp(-\mathrm{i}\varepsilon_i^{\mathrm{He}}t) \\ & + \sum_{i=N_\mathrm{T}+1}^{N_\mathrm{T}+N_\mathrm{P}} a_i(t)\frac{1}{\sqrt{2}}[\phi_{i_1}^{\mathrm{He}^+}(\boldsymbol{r}_{1\mathrm{T}})\phi_{i_2}^{\mathrm{H}}(\boldsymbol{r}_{2\mathrm{P}})w^{\mathrm{T}}(\boldsymbol{r}_1, t)w^{\mathrm{P}}(\boldsymbol{r}_2, t) \\ & + \phi_{i_1}^{\mathrm{He}^+}(\boldsymbol{r}_{2\mathrm{T}})\phi_{i_2}^{\mathrm{H}}(\boldsymbol{r}_{1\mathrm{P}})w^{\mathrm{T}}(\boldsymbol{r}_2, t)w^{\mathrm{P}}(\boldsymbol{r}_1, t)]\exp[-\mathrm{i}(\varepsilon_{i_1}^{\mathrm{He}^+} + \varepsilon_{i_2}^{\mathrm{H}})t]\end{aligned} \tag{A3}$$

where T and P refer to the helium nucleus and the proton, respectively. The factors

$$w^{\mathrm{T}}(\boldsymbol{r}, t) = \exp[-\mathrm{i}(\tfrac{1}{2}\boldsymbol{v}\cdot\boldsymbol{r} + \tfrac{1}{8}v^2 t)] \tag{A4}$$

and

$$w^{\mathrm{P}}(\boldsymbol{r}, t) = \exp[-\mathrm{i}(-\tfrac{1}{2}\boldsymbol{v}\cdot\boldsymbol{r} + \tfrac{1}{8}v^2 t)] \tag{A5}$$

are the usual plane-wave translation factors (Bates and McCarroll 1958), ensuring the Galilean invariance of the model. In the present work only singlet states of helium are considered. Therefore, Φ is symmetric under the interchange of the electronic coordinates.

As the helium wavefunctions, ϕ_i^{He}, are of CI type (Fritsch and Lin 1988), the general form of the two-electron matrix elements to be computed is

$$\langle\phi^{\mathrm{a}}(\boldsymbol{r}_{1\mathrm{A}})\phi^{\mathrm{b}}(\boldsymbol{r}_{2\mathrm{B}})|\exp[\mathrm{i}(\boldsymbol{v}_\mathrm{C} - \boldsymbol{v}_\mathrm{A})\cdot\boldsymbol{r}_1 + \mathrm{i}(\boldsymbol{v}_\mathrm{D} - \boldsymbol{v}_\mathrm{B})\cdot\boldsymbol{r}_2]O|\phi^{\mathrm{c}}(\boldsymbol{r}_{1\mathrm{C}})\phi^{\mathrm{d}}(\boldsymbol{r}_{2\mathrm{D}})\rangle_{\boldsymbol{r}_1, \boldsymbol{r}_2} \tag{A6}$$

where a, b, c and d label one-electron wavefunctions and A, B, C and D correspond to the nucleus on which they are centred. Also $\boldsymbol{v}_\mathrm{P} = \frac{1}{2}\boldsymbol{v}$ and $\boldsymbol{v}_\mathrm{T} = -\frac{1}{2}\boldsymbol{v}$ and O is any one of the operators which form the Hamiltonian (A1).

These matrix elements are six-dimensional integrals over the electronic coordinates and could be treated as standard molecular integrals in the LCAO method, if there were no velocity dependent translation factors present. Even so, the standard procedure (Roothaan 1951, Rüdenberg 1951) of transforming the integral to the body-fixed coordinate system, with its z axis fixed along $\boldsymbol{R}$, and introducing prolate spheroidal coordinates, can be followed. If O is a one-electron operator, expression (A6) reduces to a product of one-electron matrix elements which can be computed using a generalization of the method of McCarroll (1961). In the case where O corresponds to the electronic repulsion, the Neumann expansion of $1/|\boldsymbol{r}_1 - \boldsymbol{r}_2|$ is employed (Rüdenberg 1951), which is the analogue, in prolate spheroidal coordinates, of the Laplace expansion in polar coordinates. A quasi-factorization of the six-dimensional integral into a product of three-dimensional integrals results, and the same methods can be employed as for the one-electron matrix elements.

References

Allan R J, Heck E L and Zurek S 1990 *Comput. Phys. Commun.* **59** 325

Ashburn J R, Cline R A, Stone C D, van der Burgt P J M, Westerveld W B and Risley J S 1989 *Phys. Rev.* A **40** 4885

Ashburn J R, Cline R A, van der Burgt P J M, Westerveld W B and Risley J S 1990 *Phys. Rev.* A **41** 2407

Bates D R and McCarroll R 1958 *Proc. R. Soc.* A **245** 175

Brower M C and Pipkin F M 1989 *Phys. Rev.* A **39** 3323

Burgdörfer J 1986 *Phys. Rev.* A **33** 1578

Cheshire I M, Gallaher D F and Taylor A J 1970 *J. Phys. B: At. Mol. Phys.* **3** 813

Cline R A, Westerveld W B and Risley J S 1990 *Phys. Rev.* A submitted

De Serio R, Gonzalez-Lepera C, Gibbons J P, Burgdörfer J and Sellin I A 1998 *Phys. Rev.* A **37** 4111

Fritsch W and Lin C D 1988 *Phys. Rev. Lett.* **61** 690

Green T A, Stanley H E and Chiang Y-C 1965 *Helv. Phys. Acta* **38** 109

Hippler R, Harbich W, Faust M, Lutz H O and Dubé L J 1986 *J. Phys. B: At. Mol. Phys.* **19** 1507

Jain A, Lin C D and Fritsch W 1987a *Phys. Rev.* A **35** 3180

—— 1987b *Phys. Rev.* A **36** 2041 (erratum 1988 *Phys. Rev.* A **37** 3611)

Kimura M and Lin C D 1986 *Phys. Rev.* A **34** 176

Kvale T J, Seely D G, Blankenship D M, Redd E, Gay T J, Kimura M, Rille E, Peacher J L and Park J T 1985 *Phys. Rev.* A **32** 1369

Lenormand J 1976 *J. Physique* **37** 699

McCarroll R 1961 *Proc. Roy. Soc.* A **264** 547

Roothaan C C J 1951 *J. Chem. Phys.* **19** 1445

Rüdenberg K 1951 *J. Chem. Phys.* **19** 1459

Shah M B and Gilbody H B 1985 *J. Phys. B: At. Mol. Phys.* **18** 899

Shah M B, McCallion P and Gilbody H B 1989 *J. Phys. B: At. Mol. Opt. Phys.* **22** 3037

Shingal R, Bransden B H and Flower D R 1987 *J. Phys. B: At. Mol. Phys.* **20** L477

—— 1989 *J. Phys. B: At. Mol. Opt. Phys.* **22** 855

Shingal R and Lin C D 1990 *J. Phys. B: At. Mol. Opt. Phys.* submitted

Sin Fai Lam L T 1967 *Proc. Phys. Soc.* **92** 67

Slim H A, Heck E L, Bransden B H and Flower D R 1990 *J. Phys. B: At. Mol. Opt. Phys.* **23** L611

Stier P M and Barnett C F 1956 *Phys. Rev.* **103** 896

Teubner P J O, Kauppila W E, Fite W L and Girnius R J 1970 *Phys. Rev.* A **2** 1763